Journal of Electroanalytical Chemistry 686 (2012) 32–37

Contents lists available at SciVerse ScienceDirect

Journal of Electroanalytical Chemistry

journal homepage: www.elsevier.com/locate/jelechem

Inter-particle charge transfer in TiO_2-phytate films: Generator–collector gold–gold junction transients

Liza Rassaei [a,b], Markus Herrmann [a,c], Sergey N. Gordeev [d], Frank Marken [a,*]

[a] Department of Chemistry, University of Bath, Bath BA2 7AY, UK
[b] MESA+ Institute for Nanotechnology, University of Twente, 75100 AE, Enschede, The Netherlands
[c] Department of Chemistry, Technische Universität Darmstadt, 64289 Darmstadt, Germany
[d] Department of Physics, University of Bath, Bath BA2 7AY, UK

ARTICLE INFO

Article history:
Received 23 May 2012
Received in revised form 14 September 2012
Accepted 18 September 2012
Available online 27 September 2012

Keywords:
Junction voltammetry
TiO_2 phytate
Sensor
Layer by layer assembly
Nano-particle
Electron diffusion kinetics

ABSTRACT

Self-assembled films of nanoparticulate TiO_2-phytate are prepared on a gold disc–gold disc junction electrode with approximately 6 μm inter-electrode gap. Charge diffusion dominated by inter-particle hopping of electrons is investigated (in contrast to bulk charge transport) for films immersed in 0.1 M phosphate buffer solution at pH 7 using gold–gold generator–collector voltammetry and chronoamperometry techniques. Numerical simulation based on a basic "randomly propagating" finite difference approach is employed to reveal first approximation potential-dependent apparent diffusion coefficients and apparent concentrations for electrons (D_{app} increases from 9×10^{-11} to 18×10^{-11} $m^2 s^{-1}$ and c_{app} increases from 0.2 to 37 M when going from −0.8 to −1.2 V vs. SCE). A mechanistic model for inter-particle versus intra-particle electron hopping is developed. Applications of the inter-particle charge hopping process in electrochemical sensing are suggested.

1. Introduction

Mesoporous materials with high surface area are of technological interest with numerous applications in catalysis [1], as molecular sieves [2], in separation technology [3], in gas sensors [4], batteries [5], and in energy storage [6]. Layer-by-layer preparation of thin films of mesoporous materials, for example from metal oxide nanoparticles, has been reported as a versatile assembly process [7–10]. A major factor in the function of metal oxide nanostructured films on electrodes is the efficient electronic communication between the conducting substrate and the extended internal surface of the film. Charge transport in the nanoparticle network ensures that the functionalized surface is addressable from the contact [11,12]. The mechanism of charge transport in mesoporous nanocrystalline materials such as TiO_2 is of considerable interest for improving devices such as solar cells [13,14] and for addressing the fundamental issues of charge transport in porous electronic materials [15]. The rate of electron transport through electrolyte-filled mesoporous TiO_2 films is believed to be governed mainly by the time electrons spend in localized states [16] but inter-particle hopping may also dominate in non-sintered materials with "spacer" molecules connecting the nanoparticles. The transport of electrons in mesoporous oxide materials immersed in aqueous solution occurs predominantly via diffusion due to the effective screening of macroscopic electric fields by the solution electrolyte [17–19]. Therefore a simplified diffusion model can be applied as long as the distribution of available states with applied potential is known.

Previous studies of sintered materials have suggested that electron transport is limited by multiple trapping and de-trapping processes [20]. Technically, diffusion of electrons in the electrolyte-filled TiO_2 is associated to ambipolar diffusion meaning that mobile electrons in titanium dioxide carry a cloud of counter-charges e.g. cations in the electrolyte or on the surface. The ability of electrons to diffuse through the mesoporous materials is also affected by the properties such as size of the nanoparticulate materials [21] as well as by the gap between nanoparticles, the binder molecule, and the type of the electrolyte [22]. For example, Nakade et al. showed that with the increase of film porosity to percolation threshold, the dispersive transport of electrons extends to much longer timescales [23]. Zhdanov and Kasemo [24] suggested that the observed dependence of the rate of electron diffusion in mesoporous TiO_2 on electrolyte concentration is due to different arrangements of cations near the traps occupied by an electron before and after tunneling. Here, we study the electron diffusion process in a non-sintered TiO_2-phytate film [25] using a gold–gold electrode junction [26] with an inter-electrode gap of ca. 6 μm.

* Corresponding author. Tel.: +44 1225 383694; fax: +44 1225 386231.
E-mail address: F.marken@bath.ac.uk (F. Marken).

1572-6657/$ - see front matter © 2012 Elsevier B.V. All rights reserved.
http://dx.doi.org/10.1016/j.jelechem.2012.09.022

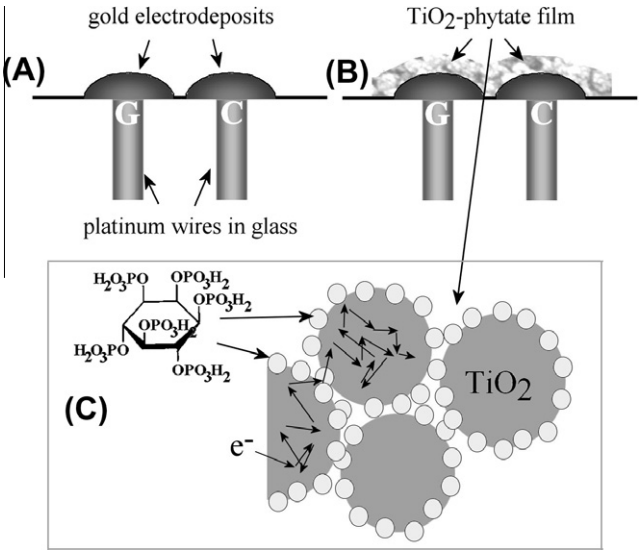

Fig. 1. Schematic drawings of (A) the gold–gold junction electrode, (B) the TiO_2-phytate film deposit, and (C) the intra- and inter-nanoparticle electron hopping process.

Paired electrodes in junctions with two independent electrodes in close proximity and under bipotentiostatic potential control are most usefully employed in voltammetric and chronoamperometric experiments. Fast diffusion processes within this junction are driven by opposite potentials applied to the generator and collector termini of the junction. These electrodes allow reaction intermediates to be investigated [27], electroanalytical processes to be enhanced [28], and local pH to be modulated [29]. Fabrication of gold–gold junction electrodes can be based on simultaneous metal electrodeposition [30], which offers a simpler "lab-bench" approach when compared for example to modern lithography techniques [31,32]. The small gap between the two electrodes (see Fig. 1) in this study is shown to provide access to the apparent diffusion coefficient D_{app} for electrons in TiO_2-phytate mesoporous films as a function of applied potential. Due to the dominating contribution of *inter-particle hopping* in contrast to *intra-particle hopping* the D_{app} value may be extracted and employed to probe the inter-particle space (see Fig. 1C).

The schematic depiction in Fig. 1C indicates the fast charge diffusion within particles with only rare hopping events between particles. This inter-particle space dependent process could be suitable for future applications in sensing where adsorption of analyte or pH changes lead to significant structural changes within the inter-particle gap and therefore to associated changes in the generator–collector current responses. In this report a first attempt is made to quantify the inter-particle electron hopping process in TiO_2-phytate films and to speculate about nano-electromechanical effects.

2. Experimental details

2.1. Chemical reagents

Potassium hydroxide, potassium gold(I)dicyanide, potassium cyanide, potassium dihydrogen phosphate, dipotassium hydrogen phosphate, potassium carbonate, poly-(diallyl-dimehtylammonium chloride) or PDDAC, potassium chloride, phytic acid, (all Sigma–Aldrich) were obtained commercially in analytical grade and used without further purification. Titanium dioxide (ca. 6 nm diameter, anatase sol. TKS-202, 30–37% acidified with nitric acid, Tayca Crop., Osaka, Japan) was a gift. All solutions were prepared using deionized and filtered water taken from an ELIX Millipore system with a resistivity of not less than 18 MΩ cm. Argon (Pure shield, BOC) was employed for de-aeration of electrolyte solutions. All experiments were carried out at 20 ± 2 °C.

2.2. Instrumentation

A PGSTAT30 bipotentiostat system (Eco Chemie, The Netherlands) was employed to control potentials at working electrodes during voltammetry and chronoamperometry experiments with a saturated calomel reference electrode (SCE, Radiometer) and a platinum gauze counter electrode. The working electrode was a gold–gold junction prepared as described below. Scanning electron microscopy (SEM) images were obtained with a JEOL JSM6310 system. Samples were gold sputter coated prior to taking images.

2.3. Procedure for fabrication of gold electrode junction

The gold–gold junction electrode was prepared following a literature method [33]. In brief, two platinum wires (100 μm diameter, approximately 12 cm long) were fed into two glass capillary tubes and these then placed into a 5 mm outer diameter glass tube (approximately 10 cm long). This assembly was then heat-sealed at one end, and polished to expose the platinum discs. The bipotentiostatic electro-deposition cell was based on the two platinum disc electrodes, a gold wire counter electrode, and a SCE reference electrode. The plating solution was based on an alkaline cyanide bath. Bipotentiostatic growth of both electrodes was carried out

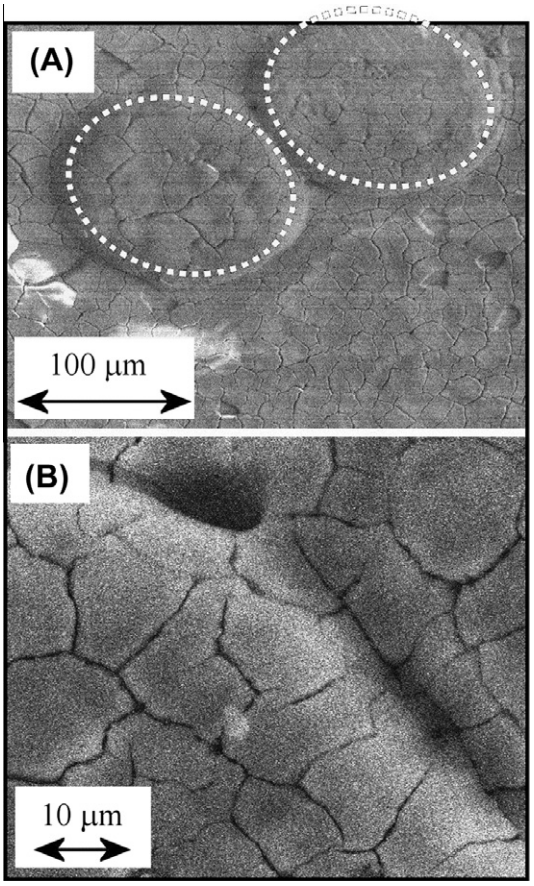

Fig. 2. Scanning electron microscope (SEM, (A) low magnification, (B) high magnification) images for a gold junction electrode covered with 100 layers of TiO_2-phytate. Crazing of film occurs after drying under vacuum conditions. Typical junction distances are in the order of 6 μm.

in a one-step process using the chronoamperometric method. One platinum disc electrode was set to a potential of −0.8800 V vs. SCE for slow gold growth. The secondary platinum disc electrode was set to a slightly more negative deposition potential of −0.8805 V vs. SCE. The difference in deposition potential was chosen small to minimize differences in the appearance of the resulting gold deposits. The automatic cut-off function (in the GPES software) was then used to stop the gold deposition process when the "cross"-current exceeded 90 μA. After the cut-off point was reached, the electrode was removed from the gold plating bath, rinsed with demineralised water, dried and tested.

2.4. Procedure for deposition of TiO_2-phytate onto the gold–gold junction

Multi-layer thin films of TiO_2 and phytate were prepared using a layer by layer assembly method [34,35] based on initial dipping the electrode into a PDDAC solution (ca. 3.5 wt.% aq.; this step is used to help initial adhesion) for 30 min followed by rinsing. The TiO_2-phytate film was formed by alternating dips into (A) a solution of 40 mM phytate (pH 3) and (B) a solution of TiO_2 nanoparticles (ca. 3 wt.%, ca. 6 nm diameter). For deposition to occur, the gold electrode junction was first dipped into the TiO_2 solution for 30 s and rinsed with water, then it was dipped into phytate solution for 30 s and rinsed with water. This procedure was repeated to build up multilayer films. For experiments described in this report a 100-layer deposit (ca. 2 μm thickness, see Fig. 2) was employed.

3. Randomly propagating finite difference simulation

The problem of two cylindrical electrodes for transient currents or approaching steady state has been treated by Seddon et al. [36] and by Amatore et al. [37]. Highly accurate calculations have been reported approaching the theoretical steady state to within 1% [37]. Here, a much more approximate but computationally convenient finite difference method is employed to allow effects from the double cylinder geometry to be accounted for, in particular in the early stages of the collector transient. Numerical simulations were carried out using MATLAB on a PC. A 2D model based on 200 × 400 boxes was used divided into eight octants with generator and collector electrodes defined circular (see Fig. 3). Concentrations were calculated explicitly:

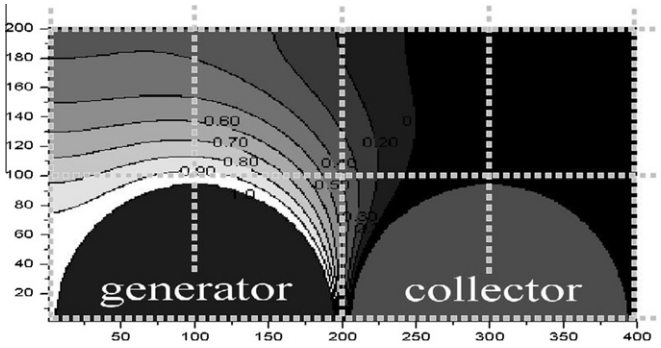

Fig. 3. Grid of 200 × 400 boxes subdivided into eight octants to exploit symmetry of circular generator and collector electrodes (top view of half electrodes). The underlying concentration gradient has been simulated for $D_{app} = 18 \times 10^{-11}$ m^2 s^{-1} for 120 μm diameter electrodes with 6 μm gap 1 s after stepping the applied potential at the generator electrode.

$$c^{t+1}[j,k] = c^t[j,k] + \frac{D\Delta t}{\Delta x^2}(-4c^t[j,k] + c^t[j-1,k] + c^t[j+1,k] + c^t[j,k-1] + c^t[j,k+1]) \quad (1)$$

Here $c^{t+1}[j,k]$ is the new concentration at time $t+1$ and at position j, k with D the diffusion coefficient, Δt the time step (0.1 ms) and Δx the box size (0.63 μm). A random number generator was employed to select the cell for the diffusion step within an octant to avoid propagation of errors (at cost of some noise). Outside boundaries were defined as closed without significant impact on the calculated currents within the first seconds of the numerical experiment.

Currents were obtained directly by separately summing all "diffusion events" within the area of the generator or collector electrodes (at the interface to the solution) and employing following equation:

$$I = 2 \times F \times \Delta c \times thickness \times \frac{\Delta x^2}{\Delta t} \quad (2)$$

Fig. 4 shows typical simulated chronoamperometry current traces for generator and collector electrodes. The collection efficiency $\left(= \frac{collector\ current}{generator\ current} \times 100\right)$ at 1 s is approximately 30% and at 15 s it reaches 90%. The simulated collector current at 15 s also approaches approximately 90% of the theoretical limiting current based on the expression given by Seddon and coworkers [36].

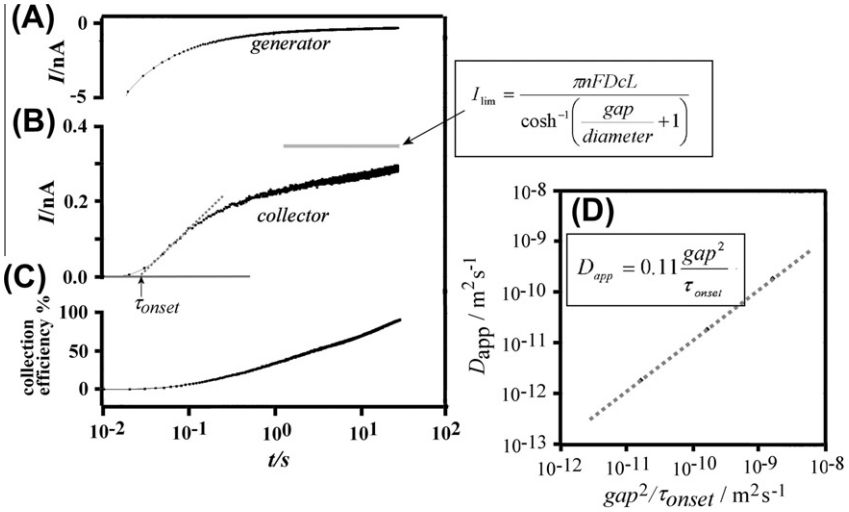

Fig. 4. (A) Simulated generator current for a chronoamperometry experiment ($D_{app} = 1.8 \times 10^{-10}$ m^2 s^{-1}; $c_{app} = 1$ mol m^{-3}) 120 μm diameter generator and collector electrodes and 6 μm gap. (B) Simulated collector current with τ_{onset} indicated and the theoretical steady state limiting current [36] indicated as a function of inter-electrode gap and electrode diameter. (C) Simulated collection efficiency. (D) Plot of the relationship between D_{app} and inverse τ_{onset} with the corresponding linear equation.

The onset of the collector current at τ_{onset} (obtained with a logarithmic time scale, see Fig. 4B) is linked to the diffusion coefficient D_{app} as shown in the plot in Fig. 4D and therefore offers an additional diagnostic tool. The noise component in the collector current is caused by the randomly propagating finite difference approach and is dominated by the region of closest approach of the two electrodes.

4. Results and discussion

4.1. Voltammetry at gold–gold generator–collector electrodes I.: $Ru(NH_3)_6^{3+/2+}$ solution redox system

Due to the complex geometric shape and method of formation of the junction electrode, the inter-electrode gap size is not very well defined. Typical gap sizes (dependent on the junction growth and cut-off conditions) are in the order of 0.1–10 μm. Solution redox systems can be employed to characterize and "calibrate" the junction electrode independently prior to further use. Here, the reduction of $Ru(NH_3)_6^{3+}$ in aqueous 0.1 M KCl is employed (see Eq. (3)).

$$Ru(NH_3)_6^{3+}(aq) + e^- \rightleftharpoons Ru(NH_3)_6^{2+}(aq) \quad (3)$$

Typical cyclic voltammetry current responses are shown in Fig. 5 for reduction of 1 mM $Ru(NH_3)_6^{3+}$ at the generator and the back-oxidation at the collector. A quasi-steady state reduction with a half wave potential of ca. −0.18 V vs. SCE is observed with a capacitive current component only on the generator current. Current signals at the collector electrode are less sensitive to the scan rate due to the highly localized inter-electrode diffusion process.

4.2. Voltammetry at gold–gold generator–collector electrodes II.: TiO_2-phytate film redox system

TiO_2-phytate self-assembled films are of interest in sensors [38] and thin film electrode applications [39]. The ability of electrons to diffuse through this nanocomposite material is affected by the properties (and size) of the nanoparticulate material as well as by the gap between nanoparticles, the binder molecule, and the type of the electrolyte. A layer-by-layer process was employed to build up thin films of TiO_2 nanoparticles (ca. 6 nm diameter) and phytate binder molecules. Here electron diffusion in these films is investigated with a gold–gold junction electrode.

Typical SEM images for a layer by layer film of TiO_2-phytate nano-composite (100 layers) in a gold–gold junction electrode are shown in Fig. 2. It can be seen that the generator–collector system is covered by a continuous film of TiO_2-phytate (with some crazing of the film mainly outside the gap zone as shown in Fig. 2B and possibly only after drying *in vacuo*). The self-assembly process took effect in the junction which is fairly uniformly filled with the mesoporous material. Thinner films produced with a smaller number of layers proved less mechanically stable and therefore less suitable for voltammetric measurements.

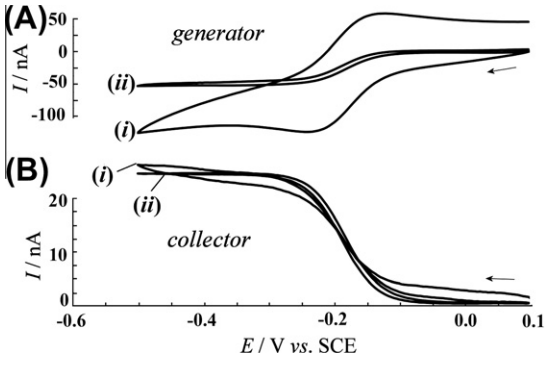

Fig. 5. Cyclic voltammograms (scan rate (i) 200 and (ii) 5 mV s^{-1}) for the reduction and back-oxidation of 1 mM $Ru(NH_3)_6Cl_3$ in 0.1 M KCl solution at a gold junction electrode. Generator currents are shown in (A) and collector currents are shown in (B).

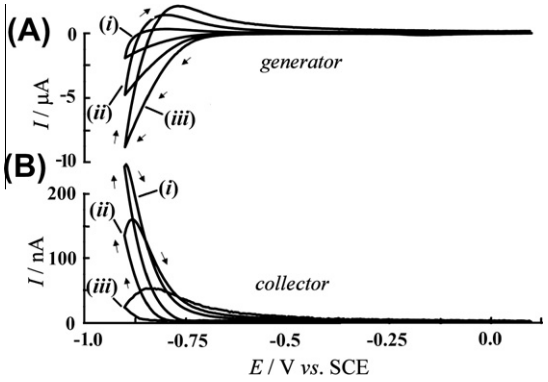

Fig. 6. Cyclic voltammograms (scan rates (i) 100 mV s^{-1}, (ii) 500 mV s^{-1}, and (iii) 2000 mV s^{-1}) for the reduction and back-oxidation of a 100 layer TiO_2-phytate film deposited into a gold–gold junction electrode and immersed in 0.1 M aqueous phosphate buffer solution pH 7. The collector electrode was biased at 0.1 V vs. SCE.

The properties of the modified gold junction electrode were first investigated by cyclic voltammetry (see Fig. 6). The generator potential was scanned from +0.1 V to −0.9 V vs. SCE with the collector electrode biased at +0.1 V vs. SCE. The onset of the reduction at the generator electrode is observed at −0.7 V vs. SCE. The onset for back-oxidation feedback current at the collector electrode is scan rate dependent.

Formally, the process of charge transport in the TiO_2-phytate film can be treated as the formation of Ti(III) close to the solid–solution interface [40] (see Eq. (4)). The chemical nature (and reversible potential) of Ti(III), however, is complicated by the fact that many types of surface sites are present and additional interaction of reduced surface sites in particular at more negative potentials cannot be ruled out.

$$Ti(IV)TiO_2 + e^- + H^+(aq) \rightleftharpoons Ti(III)(TiO_2) + H^+(TiO_2) \quad (4)$$

4.3. Chronoamperometry at gold–gold generator–collector electrodes I.: experiment

In order to develop more quantitative data analysis for junction processes (in terms of potential dependent parameters for the apparent diffusion coefficient D_{app} and the apparent concentration c_{app}), chronoamperometry methods are employed to investigate the electron diffusion process at TiO_2-phytate modified gold–gold junction electrodes. A typical chronoamperometry trace is depicted in Fig. 7. The experiment is carried out by stepping the potential to −1.0 V vs. SCE at the generator electrode while maintaining the collector at +0.1 vs. SCE. The corresponding oxidation current response is observed at the collector electrode after a short "transit" time delay.

Both the generator and the collector currents slowly converge towards a steady state current. However, after about 1 s only ca. 30% collection efficiency is reached and the system is far from steady state (compare with theory in Fig. 4). Note that transition to steady-state is expected at about $\tau_{steady-state} = \frac{(diameter+gap)^2}{D} \approx \frac{(126\times10^{-6})^2}{10^{-9}} = 15$ s. The limiting currents at 1 s are dependent on the applied generator potential. Fig. 7D shows a plot for data at generator potentials of −0.9, −1.0, −1.1, and −1.2 V vs. SCE. For more negative applied potentials both the generator and collector currents increase (see Fig. 7D) and also the corresponding collector

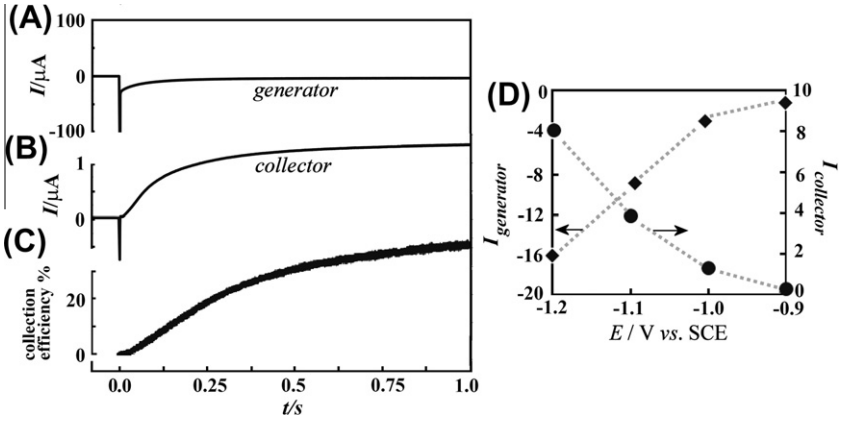

Fig. 7. Chronoamperometry data for the reduction and back-oxidation of a 100 layer TiO_2-phytate film at a gold–gold junction electrode immersed in 0.1 M aqueous phosphate buffer solution pH 7. The generator potential is stepped to −1.0 V vs. SCE and the collector potential is 0.1 V vs. SCE. Generator currents are shown in (A), collector currents in (B), and the collection efficiency in (C). (D) Plot of the currents (at 1 s) for the generator electrode (diamonds) and the collector electrode (circles) from chronoamperometry.

currents (at 1 s) increase. Due to the complex geometry, further analysis requires comparison to simulation data.

4.4. Chronoamperometry at gold–gold generator–collector electrodes II.: simulation

A comparison of experimental collector currents and simulated collector currents is shown in Fig. 8. Both the apparent diffusion coefficient D_{app} for electrons and the apparent concentration c_{app} were varied to produce good match of experiment and theory. The apparent concentration of electrons is introduced to reflect (at least in first approximation) the increase in the number of electrons per nanoparticle at more negative applied potentials (ignoring chemical changes as a function of potential). In particular for generator potentials of −0.8 V and −0.9 V vs. SCE excellent agreement is observed confirming the assumed "simple" diffusion mechanism in the presence of shielding electrolyte in pores. Perhaps surprisingly, slow electron transfer at the gold electrode – TiO_2 phytate interface appears insignificant under these conditions. For more negative generator potentials experimental current data appears impeded most likely due to additional effects including (i) the neglect of the spatial variation in D_{app}, (ii) the onset of migration effects, and (iii) chemical changes in TiO_2 particles due to increased proton intercalation at more negative potential.

The plots of the resulting data for the apparent diffusion coefficient D_{app} and the apparent concentration c_{app} as a function of generator potential are shown in Fig. 9. At the most positive potential, −0.8 V vs. SCE, the concentration c_{app} approaches 0.2 M, which is consistent with approximately 33 electrons per TiO_2 nanoparticles (estimated assuming 6 nm particles and cubic packing). Approximate empirical functional dependences of D_{app} and c_{app} on the applied generator potential E_{app} are expressed in following equations:

$$c_{app}(/\text{mol dm}^{-3}) = -350E_{app}^3 - 751E_{app}^2 - 529E_{app} - 121.68 \quad (5)$$

$$D_{app}(/\text{m}^2\,\text{s}^{-1}) = -6.43\times10^{-10}E_{app}^2 - 15.2\times10^{-10}E_{app} - 7.12\times10^{-10} \quad (6)$$

Most striking from these data is the fact that the apparent diffusion coefficient D_{app} is small and it varies only slightly over a wide range of applied potentials (in contrast to observations in sintered or bulk TiO_2 [41]). Although additional factors such as the spatial dependence of D_{app} and the effects of de-trapping and interfacial electron transfer kinetics are ignored here, it can be suggested that in contrast to more dense mesoporous TiO_2 materials, the charge hopping in TiO_2-phytate films is likely to be limited by inter-particle hopping (see Fig. 1C). This situation is similar to that observed for example in films containing molecular redox systems, which have been extensively studied for example on

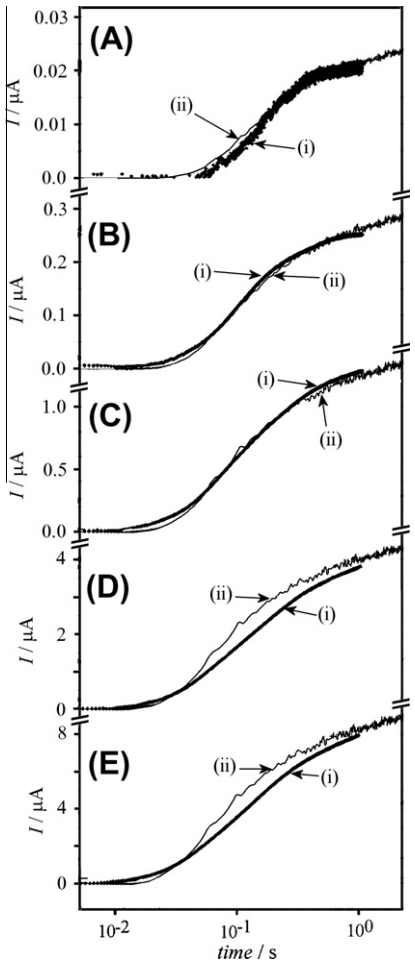

Fig. 8. Chronoampereomotry results (only collector currents shown) for the reduction and back-oxidation of a 100-layer TiO_2-phytate film at a gold–gold junction electrode immersed in 0.1 M aqueous phosphate buffer solution pH 7 for generator potentials of (A) −0.8 V, (B) −0.9 V, (C) −1.0 V, (D) −1.1 V, and (E) −1.2 V vs. SCE and a collector potential of 0.1 V vs. SCE. The experimental data (i) are compared to simulation data (ii).

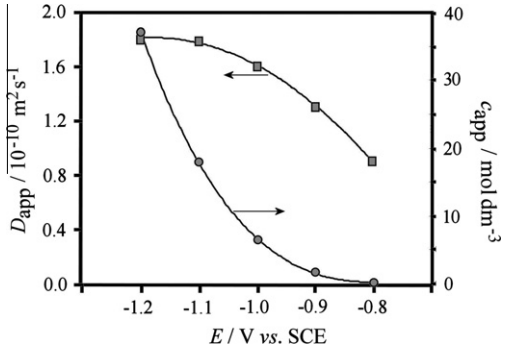

Fig. 9. Plot of D_{app} and c_{app} (from simulation of chronoamperometry collector currents, see above) versus the applied generator potential.

inter-digitated band electrodes [42]. With this assumption, it is possible to formally apply the Dahms–Ruff model [43–45] for the evaluation of the self-exchange rate constant k_{SE} (see Eq. (7)).

$$k_{SE} = \frac{6D_{app}}{\delta^2 c_{nanoparticle}} \quad (7)$$

In this equation the apparent diffusion coefficient, here $D_{app} = 1.8 \times 10^{-10}\ m^2\ s^{-1}$, the inter-nanoparticle spacing, ca. $\delta = 6$ nm, and the approximate nanoparticle concentration in the film, $c_{nanoparticle} = 6$ mM, are combined to give $k_{SE} = 5 \times 10^6\ mol^{-1}\text{-}m^3\ s^{-1}$. This implies an approximate self-exchange exchange of electrons between TiO_2 nanoparticles of $k_{SE} \times c_{nanoparticle}/6 = 5 \times 10^6\ s^{-1}$ for each inter-particle gap (assuming six close neighbors for each particle). The self-exchange frequency is likely to be linked to "Brownian rattling" due to fluctuations in the surrounding water phase causing ("nano-electromechanical") transfer of electrons to be coupled to relative inter-particle movements [46].

There are many aspects of the mechanistic understanding of the charge hopping transport in mesoporous TiO_2-phytate material that need further investigation. Further experiments as a function of both generator and collector potential are required to confirm the limitations of the simple mechanistic picture developed here. More crucially, additional experiments in which the inter-nanoparticle gap space is modified (with better binder systems and by analyte adsorption, pH variation, temperature, or dielectric constant change, electrolyte concentration variation, etc.) are desirable for the development of sensor applications.

5. Conclusion

A gold–gold junction electrode with small inter-electrode gap has been employed to explore charge hopping conduction in mesoporous TiO_2-phytate. A thin film of ca. 2 μm thickness allowed thin film conditions to be applied thereby simplifying the geometry to the case of diffusion between two cylinder electrodes. Chronoamperometry data for the collector current was adequately modeled to give a set of approximate apparent diffusion coefficients and charge carrier concentrations. There are obvious short-comings in this treatment such as the lack of spatial variation in D_{app} and ignoring effects of interfacial electron transfer or migration. Improved simulation methods as well as more experiments (variation of both generator and collector potentials, investigation of the effect of film thickness, use of more stable films) are possible and important to further explore/exploit inter-nanoparticle electron transfer. Most interesting from the experimental point of view appears to be the insight into the inter-nanoparticle gap behavior. Applications in sensing can be envisaged with collector currents providing information about environmental parameters and receptor molecules bound into the inter-nanoparticle spaces.

Acknowledgment

L.R. gratefully acknowledges the financial support from EPSRC (EP/F025726/1).

References

[1] M. Alvaro, C. Aprile, M. Benitez, E. Carbonell, H. Garcia, J. Phys. Chem. B 13 (2006) 6661.
[2] J. Liu, X. Zhang, Y. Han, F.S. Xiao, Chem. Mater. 14 (2002) 2536.
[3] B. Zornoza, S. Irusta, C. Tellez, J. Coronas, Langmuir 25 (2009) 5903.
[4] B. Sun, J. Horvat, H.S. Kim, W.S. Kim, J. Ahn, G.X. Wang, J. Phys. Chem. C 114 (2010) 18753.
[5] Y.F. Shi, B.K. Guo, S.A. Corr, Q.H. Shi, Y.S. Hu, K.R. Heier, L.Q. Chen, R. Seshadri, G.D. Stucky, Nano Lett. 9 (2009) 4215.
[6] G.R. Li, Z.P. Feng, Y.N. Ou, D.C. Wu, R.W. Fu, Y.X. Tong, Langmuir 26 (2010) 2209.
[7] G. Decher, J.B. Schlenoff, Multilayer Thin Films, Wiley-VCH, Weinheim, 2003.
[8] L. Rassaei, M. Sillanpää, E.V. Milsom, X.H. Zhang, F. Marken, J. Solid State Electrochem. 12 (2008) 747.
[9] J.L. Gunjakar, T.W. Kim, H.N. Kim, I.Y. Kim, S.J. Hwang, J. Am. Chem. Soc. 133 (2011) 14998.
[10] J.S. Lee, J. Cho, C. Lee, I. Kim, J. Park, Y.M. Kim, H. Shin, J. Lee, F. Caruso, Nat. Nanotechnol. 2 (2007) 790.
[11] A. Fattori, L.M. Peter, H.X. Wang, H. Miura, F. Marken, J. Phys. Chem. C 114 (2010) 11822.
[12] B.C. O'Regan, F. Lenzmann, J. Phys. Chem. B 108 (2004) 4342.
[13] E. Guillen, L.M. Peter, J.A. Anta, J. Phys. Chem. C 115 (2011) 22622.
[14] J. van de Lagemaat, K. Zhu, K.D. Benkstein, A.J. Frank, Inorg. Chim. Acta 361 (2008) 620.
[15] J. Bisquert, A. Zaban, Appl. Phys. A-Mater. 77 (2003) 507.
[16] P.T. Hsiao, Y.J. Liou, H.S. Teng, J. Phys. Chem. C 115 (2011) 15018.
[17] N. Kopidakis, E.A. Schiff, N.G. Park, J. van de Lagemaat, A.J. Frank, J. Phys. Chem. B 104 (2000) 3930.
[18] K. Schwarzburg, F. Willig, J. Phys. Chem. B 103 (1999) 5743.
[19] C.Y. Cummings, F. Marken, L.M. Peter, K.G.U. Wijayantha, A.A. Tahir, J. Am. Chem. Soc. 134 (2012) 1228.
[20] P.T. Hsiao, Y.L. Tung, H.S. Teng, J. Phys. Chem. C 114 (2010) 6762.
[21] A. Ofir, S. Dor, L. Grinis, A. Zaban, T. Dittrich, J. Bisquert, J. Chem. Phys. 128 (2008) 064703.
[22] S. Kambe, S. Nakade, T. Kitamura, Y. Wada, S. Yanagida, J. Phys. Chem. B 106 (2002) 2967.
[23] S. Nakade, S. Kambe, T. Kitamura, Y. Wada, S. Yanagida, J. Phys. Chem. B 105 (2001) 9150.
[24] V.P. Zhdanov, B. Kasemo, J. Phys.-Cond. Matter 1 (6) (2004) 2625.
[25] F. Marken, S.M. Parkhouse, L.A. Hoe, K.J. McKenzie, R.J. Mortimer, S.J. Vickers, N.M. Rowley, Indian J. Chem. A-Inorg. Bio-Inorg. Phys. Theor. Anal. Chem. 42 (2003) 782.
[26] S.E.C. Dale, A. Vuorema, E.M.Y. Ashmore, B. Kasprzyk-Horden, M. Sillanpää, G. Denuault, F. Marken, Chem. Rec. 12 (2012) 143.
[27] R.W. French, A.M. Collins, F. Marken, Electroanalysis 20 (2008) 2403.
[28] L. Rassaei, R.W. French, R.G. Compton, F. Marken, Analyst 134 (2009) 887.
[29] L. Rassaei, F. Marken, Anal. Chem. 82 (2010) 7063.
[30] R.W. French, F. Marken, J. Solid State Electrochem. 13 (2009) 609.
[31] L. Rassaei, P.S. Singh, S.G. Lemay, Anal. Chem. 83 (2011) 3974.
[32] L. Rassaei, K. Mathwig, E.D. Goluch, S.G. Lemay, J. Phys. Chem. C (2012), http://dx.doi.org/10.1021/jp2118696.
[33] R.W. French, S.N. Gordeev, P.R. Raithby, F. Marken, J. Electroanal. Chem. 632 (2009) 206.
[34] K.J. McKenzie, F. Marken, Langmuir 19 (2003) 4327.
[35] K.J. McKenzie, F. Marken, M. Oyama, C.E. Gardner, J.V. Macpherson, Electroanalysis 16 (2004) 89.
[36] B.J. Seddon, H.H. Girault, M.J. Eddowes, W.F. Peng, Z.F. Zhao, J. Chem. Soc. Faraday Trans. 87 (1991) 2603.
[37] C. Amatore, A.I. Oleinick, I.B. Svir, J. Electroanal. Chem. 553 (2003) 49.
[38] C. Mercado, Z. Seeley, A. Bandyopadhyay, S. Bose, J.L. McHale, Acs. Appl. Mater. Inter. 3 (2011) 2281.
[39] S.N. Britvin, A. Lotnyk, L. Kienle, S.V. Krivovichev, W. Depmeier, J. Am. Chem. Soc. 133 (2011) 9516.
[40] E.V. Milsom, H.R. Perrott, L.M. Peter, F. Marken, Langmuir 21 (2005) 9482.
[41] J. Bisquert, Phys. Chem. Chem. Phys. 10 (2008) 49.
[42] R.W. Murray (Ed.), Molecular Design of Electrode Surfaces, Wiley, New York, 1992.
[43] H. Dahms, J. Phys. Chem. 72 (1968) 362.
[44] I. Ruff, V.J. Friedrich, K. Demeter, K. Csillag, J. Phys. Chem. 75 (1971) 3303.
[45] C.Y. Cummings, J.D. Wadhawan, T. Nakabayashi, M. Haga, L. Rassaei, S.E.C. Dale, S. Bending, M. Pumera, S.C. Parker, F. Marken, J. Electroanal. Chem. 657 (2011) 196.
[46] A.V. Moskalenko, S.N. Gordeev, O.F. Koentjoro, P.R. Raithby, R.W. French, F. Marken, S. Savelev, Phys. Rev. B 79 (2009) 241403.